Using Baffle to Improve Axial Mixing in Double Cone Blenders: Dry Impregnation Process

By

AMAN RASTOGI

A thesis submitted to the

School of Graduate Studies

Rutgers, The State University of New Jersey

In partial fulfillment of the requirement

For the degree of

Master of Science

Graduate Program in Chemical and Biochemical Engineering

Written under the direction of

Maria S. Tomassone

And approved by

_____

_____

_____

New Brunswick, New Jersey

October 2018

ABSTRACT OF THE THESIS

Using Baffle to Improve Axial Mixing in Double Cone Blenders: Dry Impregnation Process

By Aman Rastogi

Thesis Director:

Prof. Maria S. Tomassone

Mixing is used in various processes across the industry and is an important operation to control the quality of products in particle processes. Rotary blenders are widely used for the mixing and dry impregnation operations and it has been understood from previous research that in such blenders the time scales for axial mixing were significantly larger than for radial mixing. The goals of this work are to understand how baffles affect the mixing process in a rotating vessel and to develop a method to determine the optimum baffle size and position to be used in a double cone vessel. To increase the extent of axial mixing, baffles that break the line of symmetry along the axis (three along the cylindrical section and two along the conical sections of the double cone) were considered. In this work we use Discrete Element Method (DEM) simulations to study systematically the effect of baffles on the axial mixing and dry impregnation in the double cone blender. The effect of different properties of baffles, e.g. height, position, angle of orientation of baffles with the various process parameters, e.g. fill level, particle size, rotation speed on the mixing

performance were studied. To measure the degree of mixing we use the Kramer mixing index, which is based on the distance between the volume centers of an axially segregated system, was calculated to quantify the mixing of the system. Simulation results show that there is an optimal baffle height for low fill levels, beyond which the mixing performance declines. The angle of orientation has little to no effect on mixing performance for large particles, whereas for smaller particles, there is an optimum range of operation. Also, results for the baffle position indicated that it affects mixing significantly more at lower fill levels, and an optimum baffle position could be found. We determined the positions in the double cone for which the particle velocity is maximum. Our proposed hypothesis is that if the baffles are located in the position of maximum velocity, they will tend to break the flow and offer best mixing performance. We observe that baffles considerably increase homogeneity in the impregnation process, but we do not observe significant differences between mixing performance for different baffle positions.

Acknowledgement

I would like to thank my thesis advisor, Prof. Maria S. Tomassone for her academic guidance, understanding and support throughout my graduate studies. I would like to thank my committee members Dr. Nina Shapely and Dr. Haoran Zhang for being part of my thesis committee. I would like to acknowledge Yangyang for being an excellent mentor, for all her technical support and her patience in teaching me all the precious lab techniques. I would like to thank everyone in the Chemical and Biochemical Engineering Department (CBE). I would like to thank my friends and roommates for keeping me motivated during my work.

Lastly, I am grateful to my mother, father, and sisters whose support as always, plays a major role in my achievements. This would not have been possible without you.

Table of Contents

List of Tables

List of Figures

Chapter 1 Introduction

Mixing is arguably the most important part of any process in the manufacturing industry. The uniform mixing of solids is crucial due to various reasons such as chemical reactions between the particles (e.g. in batteries)[1], mechanical properties of the product (e.g. spatial distribution of different particles in concrete)[2] or dosage (in solid drugs)[3, 4] etc. One such process is the dry impregnation of active metals onto a catalyst.

In the manufacture of hydrotreating catalysts, the impregnation of active metals onto a porous catalyst support is a crucial step that ultimately may determine the activity and selectivity of the resulting catalysts. In this process, metal salts or complexes are dissolved in an aqueous solution and are introduced to a porous oxide catalyst support such as alumina (Al_2O_3) or silica (SiO_2). In a typical dry impregnation (pore filling or incipient wetness impregnation) process, metal solutions are sprayed over a powder bed in a mixing vessel until the amount of solution sprayed equals 95-101% of the pore volume. During spray, capillary action draws the metal solution into the pores and metal complexes are adsorbed on to the high surface area support. The operation typically takes 30 to 60 minutes, which includes impregnation time and subsequent mixing time. After impregnation, the catalyst support is dried, calcined, and further pretreated to its desired active form.

Dry impregnation is a common process in the catalyst industry, but it has mostly been studied from a surface chemistry standpoint rather than a dynamical standpoint. Interaction between the metal and the support, the transport phenomena involved in this process and the effect of these elements on the metal content and profile within the catalyst particle has been studied in detail in [5-12].

A quality hydrotreating catalyst requires a uniformed distribution of active metal within the catalyst support, which increases the hydrogenation ability of resulting catalyst. Ideally, the granular catalyst support should be introduced to a homogeneous distribution of metal solution, thus maintaining an adequate content uniformity; however, in practice this is exceedingly difficult. In addition, the blender geometry may exhibit poor directional mixing, dead zones, or particle segregation, each further reducing the desired content uniformity. The common solution is to simply blend for longer time; however, this may cause unnecessary attrition of the catalyst support. Therefore, the ability to adequately mix the powder bed, while simultaneously achieving a uniform distribution of fluid is of fundamental importance and a considerable challenge.

The cost of poor mixing was estimated at $1 billion to $10 billion in the U.S. chemical industry alone [13]. Despite a lot of research having been done in this space it is still difficult to design a mixing process with these principles due to incomplete knowledge of the mixing mechanism. Numerous types of mixers have been developed for mixing granular mixtures of which v-blenders and double cone are widely popular in the industry because of their efficiency. In this study we use a double cone blender for the impregnation process. In previous studies on tumbling blenders [14-17], the flow regime has been carefully characterized into cascading, avalanching and cataracting, etc. The mechanisms of segregation and mixing have also been analyzed. A number of studies have been performed on mixing behavior in the double cone blender which investigate the mixing and flow mechanisms[18-23]. These studies show that radial mixing is extremely fast as compared to the axial mixing in a double cone and hence is the bottleneck for the mixing process. It is also known that axial diffusion and dispersion coefficients increase with

increasing particle size [16, 17]. It was then found by Muzzio *et al.*in [24] that the mixing within two halves of the double cone blender is much faster than the mixing across the line of symmetry. It was then suggested and proved by Muzzio et al. [24] that an axial deflector plate significantly increases axial mixing in a double cone blender. Tomassone *et al.*[25, 26] study the catalyst impregnation process in the double cone blender with alumina catalyst beads. By combining both DEM simulations and experimentation they also show that axial mixing is the limiting factor to achieve homogeneity within the particle bed.

The objective of this study is to determine how baffles affect the mixing and the impregnation process in a rotating vessel and to develop a method to determine the optimum baffle position, size, orientation and shape to be used to increase the extent of axial mixing in a double cone vessel. There has been considerable amount of research to study how baffles can be used to improve mixing in double cone blenders as well as other geometries [27-38]. The problem however is that baffles are very specific to the type of particles and geometry that they are being incorporated in, hence in this case, it is tricky to use empirical results from other studies to guide our research. In this study we perform an empirical study to find the effect of different process and baffle parameters on mixing performance and then analyze the granular flow to gain further insight into why these effects happen.

Chapter 2 - Methodology

2.1 Discrete Element Method

In this work Discrete Element Method (DEM) was used to perform all particulate simulations since it gives very detailed information about the flow and state of the particles over time. DEM is increasingly being used to simulate particulate material and systems where complex physical structures and particle flows exist. In Discrete Element Method, every particle is treated as a discrete point and all the forces (body forces, contact forces, hydrodynamic forces and cohesive forces) are considered and then integrated over time to get the position and velocity of the particle. A commercially available software, EDEM™ (DEM Solutions Inc.), which is based on an original method proposed by Cundall and Strack [39], was used to design the geometry and algorithm for water transfer in the system,

DEM uses Newton's laws of motion to calculate particle trajectories and reaction forces.

$$ma = \sum F_{Contact} + \sum F_{Body}, \quad (1)$$

where m and a are the mass and acceleration of a solid particle, respectively. The term $\sum F_{Contact}$ accounts for all the normal and tangential contact forces, which are due to particle-particle or particle-boundary collisions. $\sum F_{Body}$ denotes the sum of all body forces due to gravity.

The contact forces are calculated using Hertz-Mindlin no-slip contact model. It is based on a soft contact model or elastic approach, in which the magnitude of repulsive force is related of the amount of overlap. The normal force is calculated using a damped Hertzian

normal contact [40] model with the damping term given by Tsuji et al.[41]. The magnitude F^n from a contact that resulted in a normal overlap δ_n is given by:

$$F^n = -k_n \delta_n^{3/2} - \gamma_n \dot{\delta}_n \delta_n^{1/4}, \quad (2)$$

where k_n is the Hertzian normal stiffness coefficient, δ_n is the deformation (normal particle overlap), γ_n is the normal damping coefficient, and $\dot{\delta}_n$ is the rate of deformation.

In the above equation, k_n is obtained by:

$$k_n = \frac{4}{3} E_{eff} \sqrt{R_{eff}}, \quad (3)$$

where E_{eff} is the effective Young's modulus of two colliding entities (two particles or a particle and a wall). For entities with Poisson's ratios ν_1 and ν_2, Young's moduli E_1 and E_2, E_{eff} is given by:

$$E_{eff} = \frac{1-\nu_1^2}{E_1} + \frac{1-\nu_2^2}{E_2}, \quad (4)$$

where R_{eff} is defined as the effective radius of the contacting particles. In case of a particle–wall collision, the effective radius is simply the particle radius. While in the case of particle–particle collision, with the two contacting particles having radii R_1 and R_2, the effective radius is obtained by:

$$R_{eff} = \frac{R_1 \times R_2}{R_1 + R_2}. \quad (5)$$

With the knowledge of the normal stiffness coefficient and a chosen coefficient of restitution ε, the normal damping coefficient γ_n is calculated as:

$$\gamma_n = 2\sqrt{\frac{5}{3}\left[\frac{ln(\varepsilon) \times \sqrt{m k_n}}{\sqrt{ln^2(\varepsilon) + \pi^2}}\right]}, \quad (6)$$

where k_n is the Hertzian normal stiffness coefficient.

Following the work of Mindlin and Deresiewicz [42], the tangential force F^t is calculated in a similar method as its normal counterpart. The tangential contact force also consists of elastic and damping components. When a tangential overlap of δ_t is detected and there is a corresponding normal overlap of δ_n due to the same contact, then the tangential force is expressed by:

$$F^t = -k_t\delta_t - \gamma_t\dot{\delta}_t\delta_n^{1/4}, \tag{7}$$

where k_t the tangential stiffness coefficient and γ_t is the tangential damping coefficient. In the above equation, k_t is calculated by:

$$k_t = 8G_{eff}\sqrt{R_{eff}}\sqrt{\delta_n}, \tag{8}$$

where G_{eff} is the effective shear modulus. For two entities with shear moduli G_1 and G_2, G_{eff} is calculated as:

calculated as:

$$\frac{1}{G_{eff}} = \frac{2-\nu_1}{G_1} + \frac{2-\nu_2}{G_2}, \tag{9}$$

where ν_1 and ν_2 are the Poisson's ratios.

The tangential displacement (or overlap) δ_t is calculated by time-integrating the relative velocity of tangential impact, v_{rel}^t between two colliding entities (either interparticle or particle–wall contact):

$$\overrightarrow{\delta_t} = \int \overrightarrow{v_{rel}^t} dt. \tag{10}$$

The bulk material properties and the interaction properties (friction coefficients, coefficient of restitution) between particles and particles and the geometry used in the EDEM simulations are listed below.

Table 1. Particle Material Properties used in the simulations.	
Particle	
Parameter	**Value**
Density	1500 kg/m^2
Shear modulus	10^4 N/m^2
Poisson ratio	0.25
Vessel Geometry (Steel)	
Density	7800 kg/m^2
Shear modulus	$7x10^{10}$ N/m^2
Poisson ratio	0.3

Table 2. Interaction Properties used in the simulations	
Particle-Particle	
Coefficient of restitution	0.1
Coefficient of static friction	0.4
Coefficient of rolling friction	0.01
Particle-Geometry	
Coefficient of restitution	0.1
Coefficient of static friction	0.5
Coefficient of rolling friction	0.01

2.2 Water Transfer Algorithm

The capabilities of EDEM include user defined functions and various features for simulating impregnation process, which has been developed in previous work by Romanski *et al.* [25]. The fluid spray components are modeled as discrete droplets, which are sprayed from above the rotating bed and are absorbed upon contact with the simulated catalyst particles. The corresponding contact causes the simulated fluid droplet to essentially disappear while simultaneously transferring the mass of the fluid droplet to the simulated catalyst support particle, leading to a net increase in the mass. The mass flow rate of the fluid is defined as:

$$Q_{spr} = NV = N\frac{m}{\rho} \quad (11)$$

where N is the number of fluid droplets, V is the volume, m is the mass and ρ is the density of each droplet. Analogous to the experimental conditions, the particles in this study are modeled to absorb fluid up to 35% of their weight. After saturation of the catalyst particle occurs, additional fluid allows the support particles to be considered supersaturated, and as a result, they transfer any excess of fluid to any non-saturated particle that they come into contact with. The amount of fluid transferred between two particles in every contact when one of them is supersaturated, is defined as:

$$Q_{tr} = \kappa(m_i - m_j). \quad (12)$$

In the above equation, κ is a proportionality constant which reflects the rate of fluid transfer, m_i and m_j are the respective mass of each of the particles; for this work, $\kappa$was defined as 0.01. So, the amount of fluid transferred per contact is a function of the difference in the wetness of the contacting particles. When the amount of fluid absorbed is more than the fluid contained in the pore volume, the fluid transfer algorithm allows the excess of fluid on a specific catalyst support particle to be transferred to another adjacent particle at a specific rate.

2.3 Quantification of Mixing

2.3.1 Mixing Index

A mixing index is considered to quantify the mixing in the system. In this work, Kramer's mixing index [43] has been used as it is quite simple to implement considering the large amounts of data that DEM simulations generate. For a binary mixture of two types of particles *a* and *b,* Kramer's mixing index is defined by the distance between the volume centers of the two types of particles.

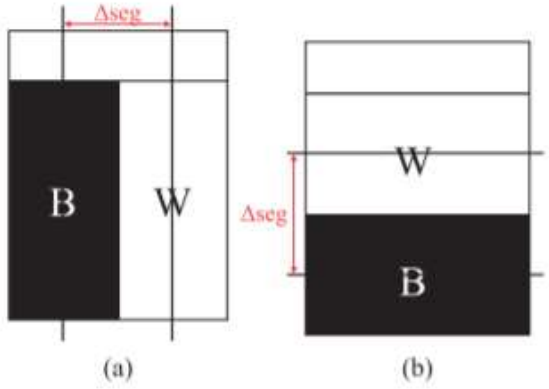

Figure 1. Kramer's mixing index. Sytems segregated in a) horizontal and b) vertical direction.

$$M = \frac{(\Delta_{seg} - \Delta_x)}{(\Delta_{seg} - \Delta_{mix})} \qquad (13)$$

Where,

Δ_{seg} is the distance between the two volume centers.

Δ_x is the distance between two volume centers after some mixing.

Δ_{mix} is the minimum possible distance between the two volume centers, which in our case is zero.

The distance is then compared to the initial and least possible distance between the volume centers. This leads to a mixing index which increases from *0* to *1*, with *M=0* being the unmixed state and M=1 being a completely mixed state. Kramer's mixing index can be used to study mixing in any particular direction. In this work, Kramer's mixing index has been used to quantify axial mixing in the double cone blender.

2.3.2 Relative Standard Deviation (RSD)

Cullen et al. [44] explained relative standard deviation (RSD) or the coefficient of variance (C_v), as another important mixing measure as follows:

$$C_v = \frac{\sigma}{\bar{C}} = \frac{\sqrt{\frac{1}{n-1}\sum_{i=1}^{n}(C_i - \bar{C})^2}}{\bar{C}}$$

Where σ is the standard deviation and $\bar{C}$ is the mean concentration for the overall samples that are analyzed. RSD is a very useful measurement to determine how the target component concentration affects mixture quality. RSD calculation is used in pharmaceutical industry where the active ingredient makes a small proportion of the mixture. In this study, RSD has been used to quantify uniformity of liquid content across the double cone impregnator.

There is not a general consensus regarding a fixed value for the for the Relative Standard Deviation (RSD) uncertainty to indicate uniformity; rather, the value of the RSD used as a threshold depends on the application and the sample size. In some cases, the observed variability is combined with the observed bias in sample average to provide a combined criterion, so that the limit in RSD actually depends on the observed level of deviation in the sample mean. The size of our samples is about 100 particles per sample in the simulations. It is standard and widely accepted to consider a 95 percent or higher confidence interval in normal distributions to have assurance of batch acceptability. Hence, we take RSD <0.1 as our criterion for a reasonably good degree of uniformity since RSD values smaller than 0.1 correspond to a 95 percent confidence interval. In addition, in general, in the catalysis industry it is widely accepted that a 10% variation in the catalyst quality is a reasonable variability, since other quality factors (surface area, activity, metals

dispersion, crush strength, etc) are often specified to this level of variation. The RSD in simulations in this study has been measured using samples from 7 bins along the axis the double cone blender similar to the way in [25]. Figure 2 shows a snapshot of the simulation where the 7 bins to take samples have been included in the figure.

Figure 2. Bins used for measuring RSD [19]

2.4 Equipment Design

Baffles are frequently used to improve mixing in systems. They represent a way to overcome any disadvantages that the existing standard designs might have. Though they are so frequently used, there has not been a lot of research towards their effect on granular flows and the ways to optimize their placement, shape etc. Around 70 simulations were run with varying baffle parameters like angle, height, width and operating parameters such as fill level, rotation speed, and particle size

Operation Parameters	
Rotation rate	5rpm, 25rpm
Fill Level	25%, 50%
Particle size (mm Diameter)	5mm, 10mm
Spray Rate	2.5 L/h
Baffle Parameters	
Size (H/R)	0.25, 0.5, 0.75, 0.9, 1.0, 1.1
Angle of orientation (deg)	0, 15, 30, 45, 60, 75
Position	1 - 5
Width (mm)	50, 75, 100, 125

Table 3: Operation Conditions and Baffle Parameters used in the simulations.

The geometry of the double cone vessel was constructed to imitate a Patterson-Kelly 10-quart rotating double cone, 24 cm in diameter and 30 cm in height, as shown in Fig. 3. Figure 3 also shows all the locations chosen for the baffles, numbered from 1 to 5. Position 3 is at the center of the double cone in the cylindrical part. Positions 2 and 4 are above and below position 3 in the edges of the cylindrical part of the double cone, and positions 1 and 2 are in the conical part of the double cone. So, the five positions of baffles are distributed as follows; three along the cylindrical part of the double cone, up, middle and down, and two positions along the conical part of the double cone, one each in the upper and bottom halves tilt-up and tilt-down.

The double cone is rotating around the y axis. Since the baffle can be placed anywhere within the double cone vessel, this gives us a very large number of possible positions to simulate. Hence, to study the effect of baffle position, we evaluate the mixing performance in five different zones mentioned above. In principle we consider only one of the sides to gain understanding on the overall effect that baffle. Notice that only one baffle per run is

used, in any of the 5 positions indicated in Figure 3. The schematic in Figure 3 shows all the positions used but only 1 baffle located in any of these positions for each run is considered

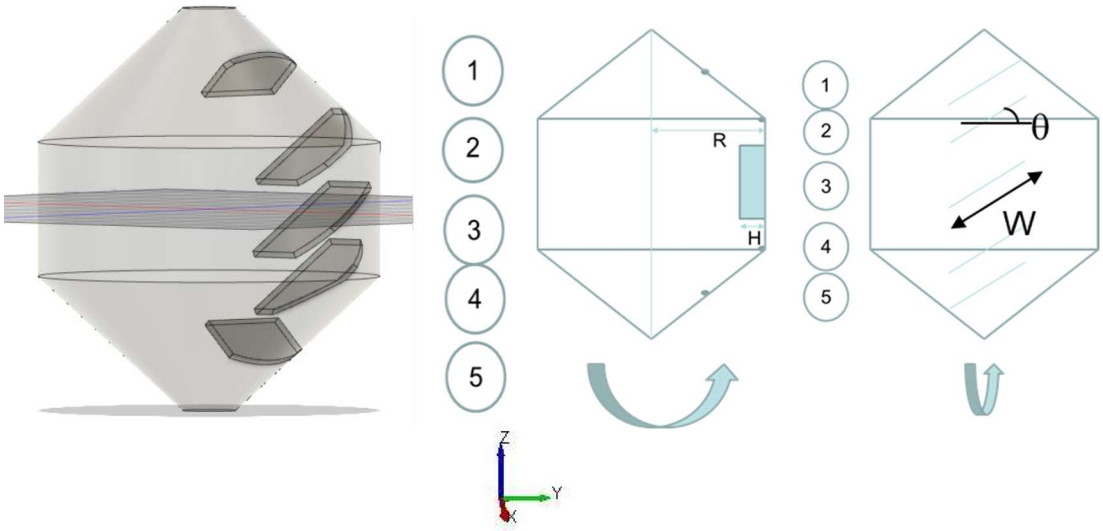

Figure 3 Schematic of different baffle positions (1-5) and direction of rotation

Figure 4. Experimental Set-up used to model simulations

Chapter 3 – Results and Discussion

3.1 Effect of Baffle Size

The effect of the size of the baffle on the mixing performance was explored. In order to do this, we considered two cases with different particle diameters: (i) 2400 particles of diameter 10 mm or (ii) 20,000 particles of diameter 5 mm. For these two cases we used to a 25% fill level in each of the simulation runs. The particles were loaded in a side-side configuration where they were axially segregated along the axis of rotation of the double cone blender (shown in Figure 5). The vessel is rotated around the y axis.

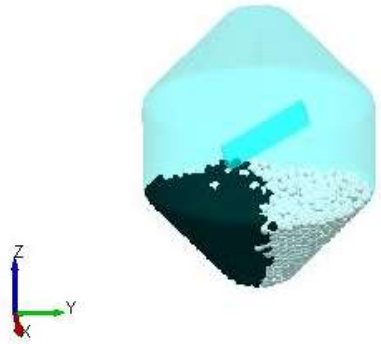

Figure 5. Simulation snapshot showing the Side-side initial loading pattern. Y axis is the axis of rotation.

The vessel was rotated at 25 rpm for both cases (i) and (ii). At this rotation rate, the flow regime was observed to be a continuous flow regime [16, 17] where there is a shear layer on top that moves freely and a core that rotates as a single unit.

The size of the baffles was characterized by the ratio H/R, where H is the height of the baffle perpendicular to the flow and R is the radius of the cylindrical part of the double cone blender as shown in Figure 3.

(i) Particles of 10 mm in diameter

For the first case we first studied the performance of a baffle in position 3, i.e. placed in the middle of the cylindrical portion of the double cone blender such that its height was perpendicular to the flow. The baffle was oriented at 30^0 with the x axis. The H/R ratios studied in this case were 0.25, 0.5, 0.75, 0.9, 1.0 and 1.1.

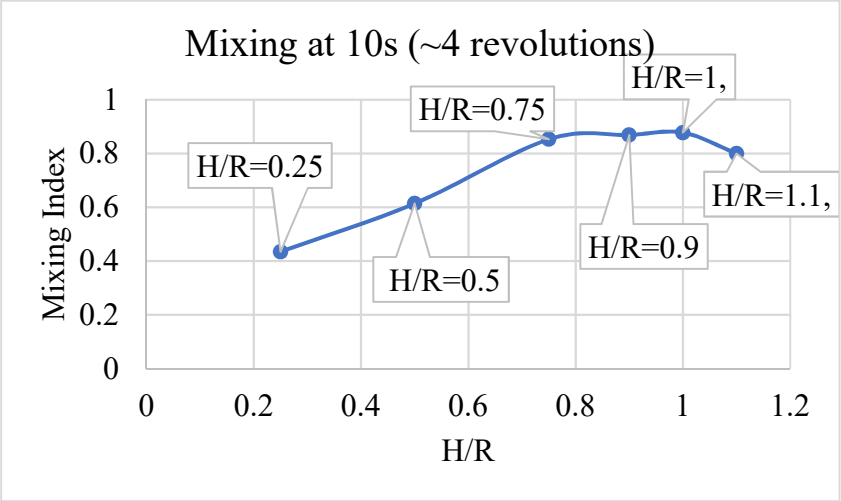

Figure 6. Mixing index at 10s for different baffle heights (H/R) ratios at 25% fill, 25rpm and 10mm particle diameter

We find that the mixing performance increases with the H/R ratio until H/R reached 1.0 and then after that value, the mixing performance starts decreasing

(ii) Particles 5 mm in diameter

The same simulations were then performed for a smaller particle size of diameter 5mm (see Fig. 7).

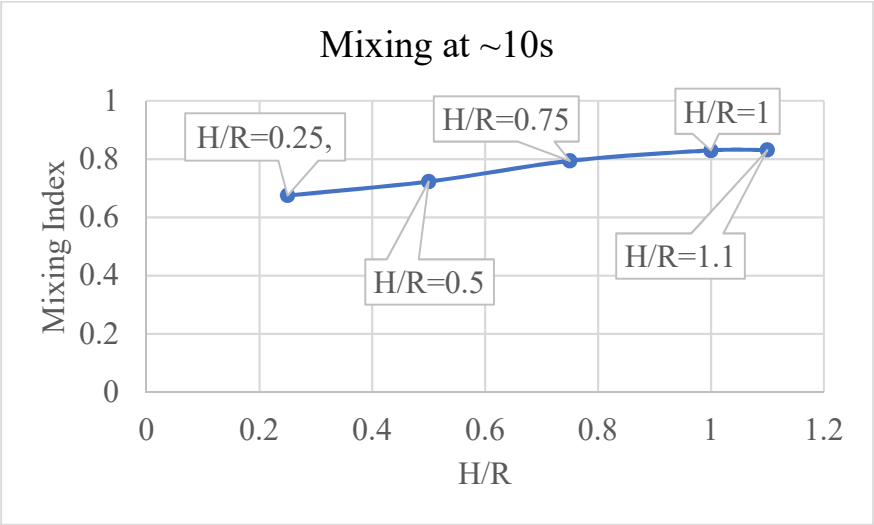

Figure 7. Mixing index at 10s for different baffle heights (H/R) ratios at 25% fill, 25rpm and 5mm particle diameter

It can be observed that there exists an optimal baffle size which offers the best mixing performance which is around H/R=1, which is the same value obtained for particles of diameter of 10mm.

Effect of width of the baffles

Also, the width of the baffle was varied from 50mm to 125mm in steps of 25mm. The results hence obtained for particles 10 mm in diameter are detailed in Fig. 7 showing Mixing Index as a function of time for different baffle widths. Although the curves are very close to each other, 50mm can be pointed out as the worst option, where mixing index is approaching 1 at the slowest rate. As the width is increased, 75mm and 100mm offer good mixing performance but it can be observed that the mixing index oscillates a little before reaching 1. At 125mm, the mixing performance is observed to be similar to 75mm and 125mm but the oscillations are very large due to the large size of the baffle which causes proportionally large movement of particles from one end to another.

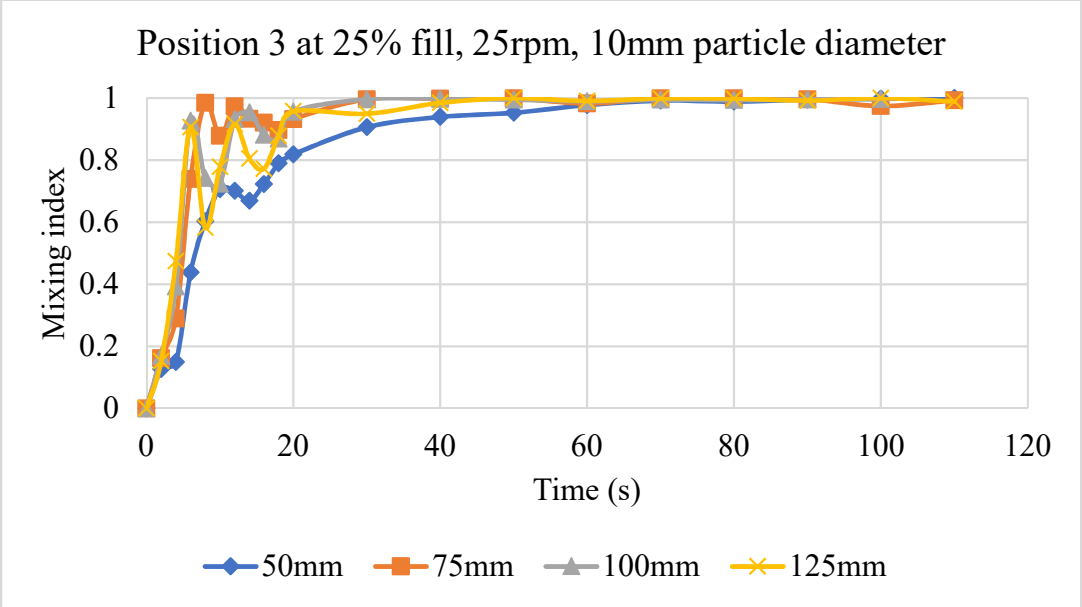

Figure 8. Variation of Mixing index with time at different baffle width

3.2 Effect of Angle of Orientation

The effect of the angle of orientation of the baffle on the mixing performance was explored. In order to do this, we also consider two different size particles, 2400 particles of 10 mm

diameter or 20000 particles of 5 mm diameter. The particles were loaded in a side-side configuration where they were axially segregated along the axis of rotation of the double cone blender. The vessel was rotated at 25 rpm. The baffles were placed at Position 2 and the angle of inclination to the z axis was changed 0 to 75 degrees in steps of 15 degrees for each change. The mixing index was then plotted against time as shown in Fig 9. We only considered position 2 because it was computationally too costly but more cases are being run to have a definitive conclusion about the orientation.

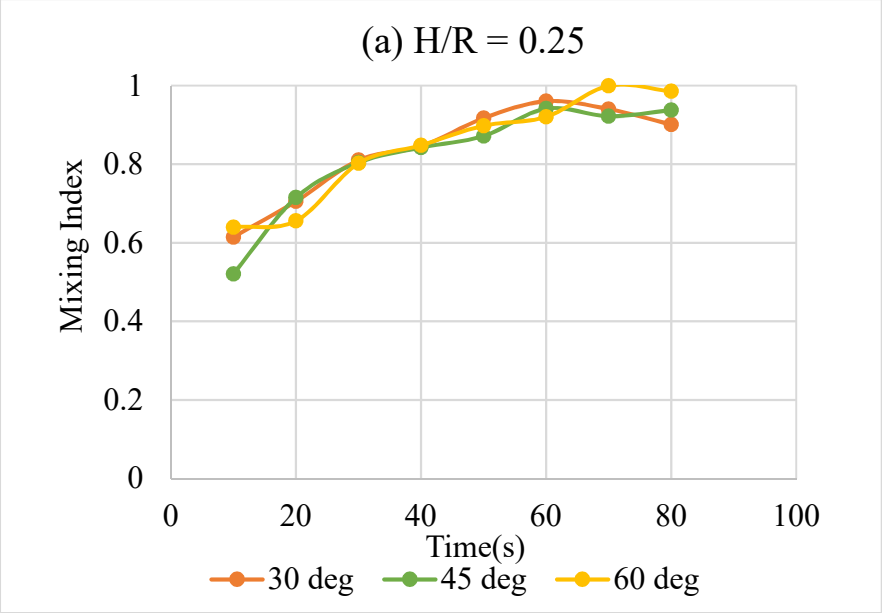

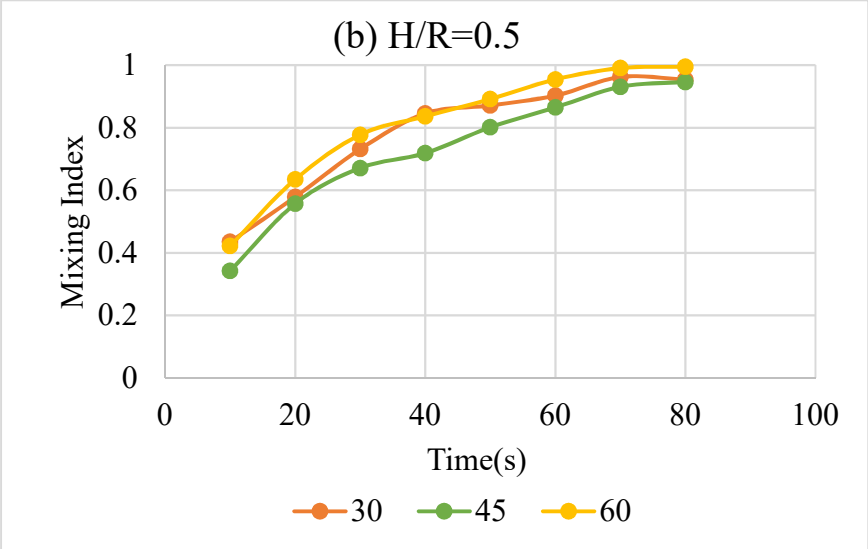

Figure 9. Mixing performance for varying angles of orientation at a) H/R=0.5 and b) H/R=0.25. The operating parameters used were 25% fill, 25rpm and 10mm particles at Position 2

When we change the angle of orientation of the baffles at a single position (Position 2), we observe that the mixing performance is not significantly affected by the angle of orientation of the baffles with respect to the x axis.

Figure 10. Mixing performance for different angle of orientation at 25% Fill, H/R=0.25, 25rpm, 5mm particles

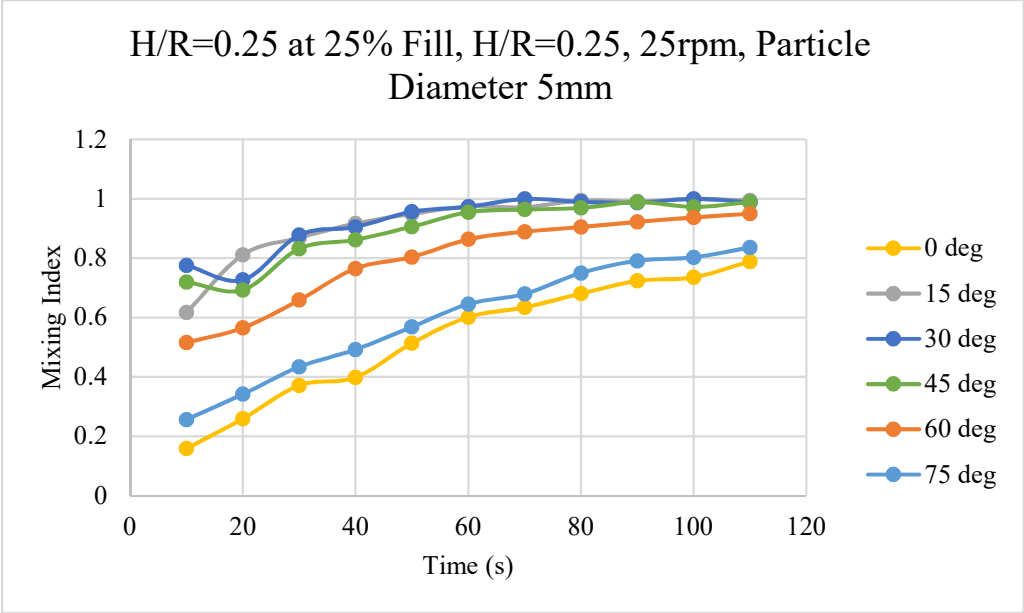

In the simulations with a smaller particle size of 5mm, we observe that the angle of orientation of the baffle has a much more significant effect on the mixing characteristics. We observe that 15 and 30 degrees offer the best mixing performance which decreases as we keep on increasing the angle of orientation. This behavior points to a balance between conservation of momentum which increases as we increase the angle and the deviation offered in the axial direction which decrease as we increase the angle. A preliminary conclusion might be suggested that for a system with two flows running parallel to one another, an optimum angle of orientation for a baffle exists such that mixing is the maximum.

3.3 Effect of Position

Since the baffle can be placed anywhere within the double cone vessel, this gives us a very large number of possible positions to examine. Hence, to study the effect of baffle position on the mixing performance, we divide the double cone into five different zones. The five positions of baffles are distributed as follows; three along the cylindrical part of the double

cone, up, middle and down, and two positions along the conical part of the double cone, one each in the upper and bottom halves tilt-up and tilt-down. The positions are described in the figure below.

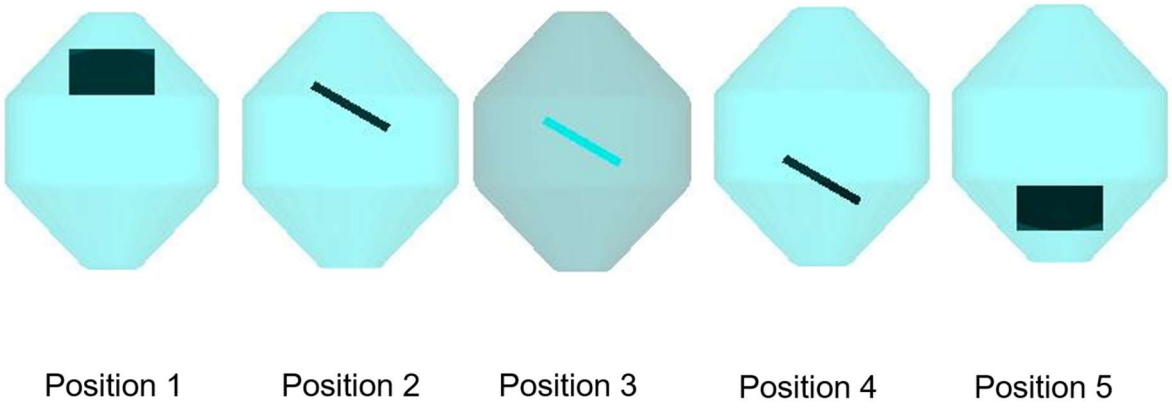

Figure 11. Simulation snapshots showing different positions of baffle

The mixing behavior is then studied for each position with respect to time. All the other conditions are kept constant and then the mixing behavior at each of the position is compared. Fig. 11 (a) displays the results from simulations at 25% fill level, H/R = 0.25 and 25 rpm rotations rate for all the positions.

(a)

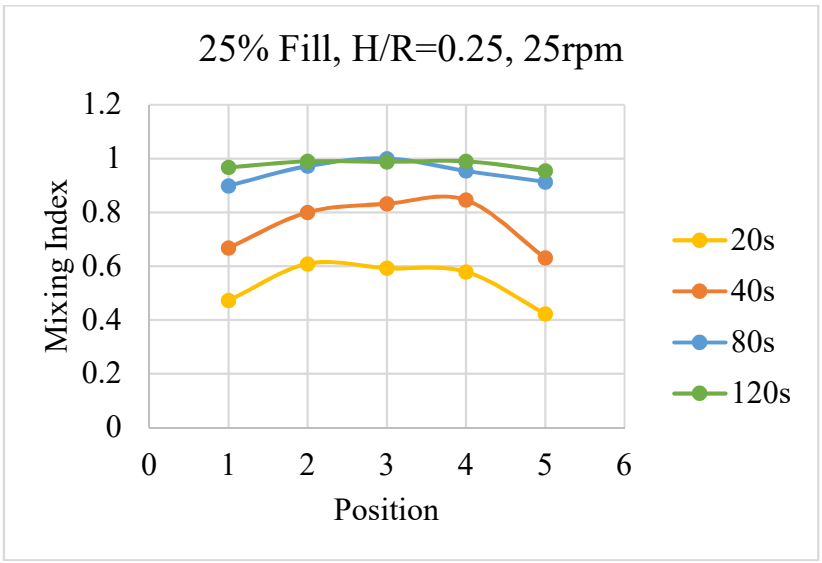

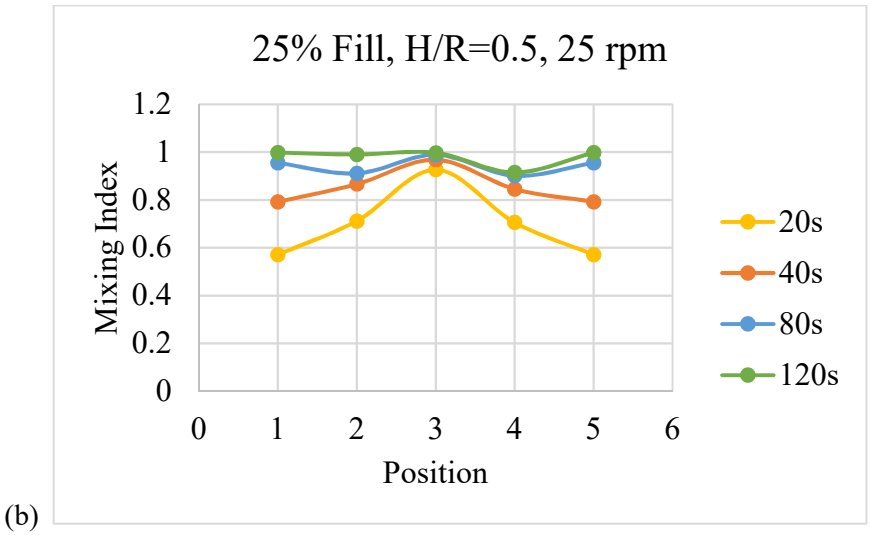

(b)

Figure 12. Mixing performance for different baffle positions at 25% Fill level and 25 rpm at a) H/R=0.25 and b) H/R=0.5.

It can be observed that the positions 2,3 and 4 display the best mixing performance, whereas positions 1 and 5 are less effective in the beginning 40 seconds of the mixing process. As more revolutions are performed, for all the positions, the system reaches good mixing at around 80s. The same set of simulations are repeated for a larger baffle size at H/R = 0.5 as displayed in Fig 11(b). At larger baffle size, a more distinguishable difference can be observed between mixing performance at different positions. Position 3 displays the best mixing performance. Positions 2 and 4 display slower mixing whereas positions 1 and 5 display the slowest mixing in the beginning stages. Eventually at 120 seconds all positions seem to perform with a high mixing index.

Since an optimum position can be found at these operating conditions, it is desirable to know whether changing the fill level has any effect on the mixing profile for different baffle positions.

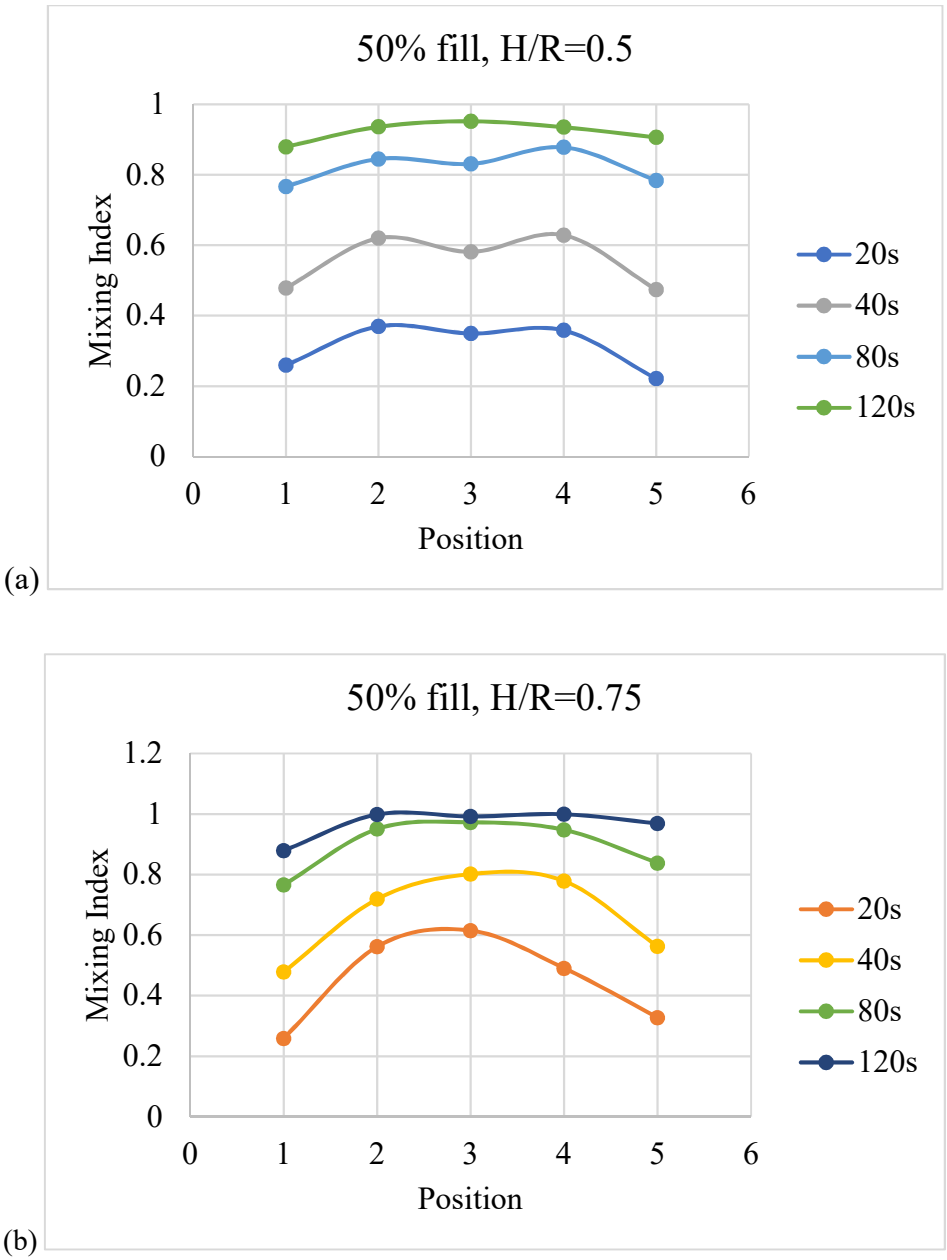

Figure 13. Effect of Position at Fill Level 50%, 25rpm, 30 degree angle at a) H/R=0.5 and b)H/R=0.75

Figure 13 and b shows the results of the effect of the baffle position for a fill level of 50% at a 30 degree angle and at two different baffle size ratios: H/R=0.5 and H/R=0.75. When the fill level is changed to 50%, we observe a similar behavior as the one found at fill level 25%. We also observe the larger the baffle size the more significant these effects become.

This suggests that the height of the particle bed at the point of contact with the baffle may play an important role in the effectiveness of the baffle. Hence a more effective representation of baffle height might be the ratio of baffle height to bed height rather than radius as a metric of baffle dimensions. But since the flow in a double cone is complex and the bed height is difficult to characterize, we will continue to use H/R as the metric for baffle height.

3.4 Effect of Rotational Speed

One of the important operating parameters to be studied in any rotary mixing vessel is the rotational speed of the vessel. We considered two different rotational speeds, 5prm and 25rpm. It is known from previous studies that higher rotation speeds lead to faster mixing [18] with respect to time, but when measured in mixing rate per revolution, the rotation rate has little effect on the mixing rate per revolution. The results are shown below in Fig 14 a and b.

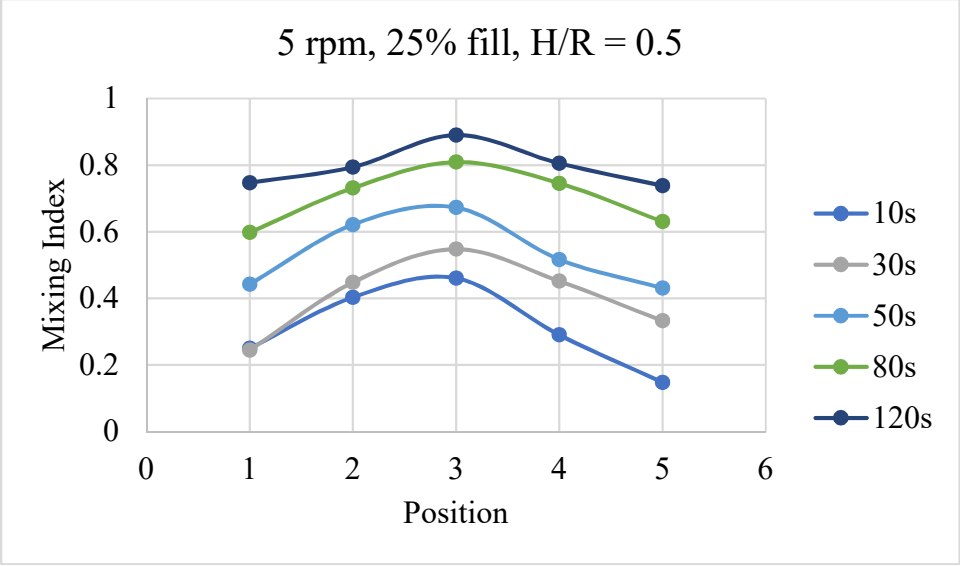

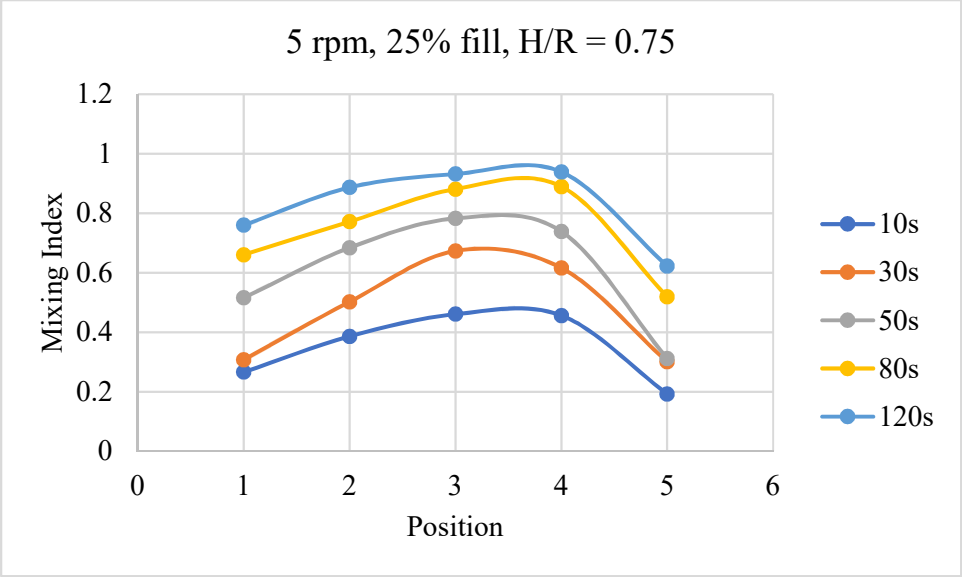

Figure 14. Mixing performance at lower rotation speed (Ω=5rpm)

Figure 14 (a) shows that the mixing behavior for baffles at lower rpm mimics that at higher rpm. The position 3 still offers the best mixing performance out of all five positions. The mixing at low rpm is slower than at high rpm as expected. The interesting thing to note here is that changing the rotation speed from 25 rpm to 5 rpm also changes the flow regime from continuous to avalanching [16, 17] but still does not affect the optimum baffle position.

3.5 Effect of Fill level

Two fill levels of 25% and 50% were tested during the study. Higher levels were not included as they lead to a sharp increase in simulation time. 2400 and 4800 particles of 10mm diameter were used to fill 25% and 50% of the vessel volume respectively. The rotation rate was kept constant at 25 rpm. The baffle was positioned either of positions 2, 3 and 4. The size of the baffle was kept constant at a ratio H/R=0.5 and the baffle was oriented at 30^0 with the x axis. Sampling was done using in 7 bins across the y axis as shown in Figure 2 Then the ratio of white to black particles was calculated and the relative

standard deviation (RSD) around a mean of 1 was calculated. The variation of RSD with time for the two fill levels and different baffle positions are shown below in Figures 15 a) and 15 b).

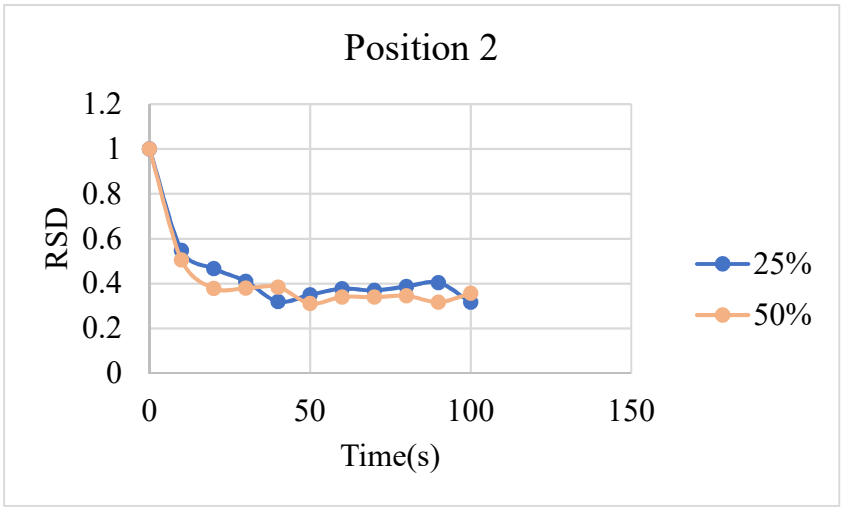

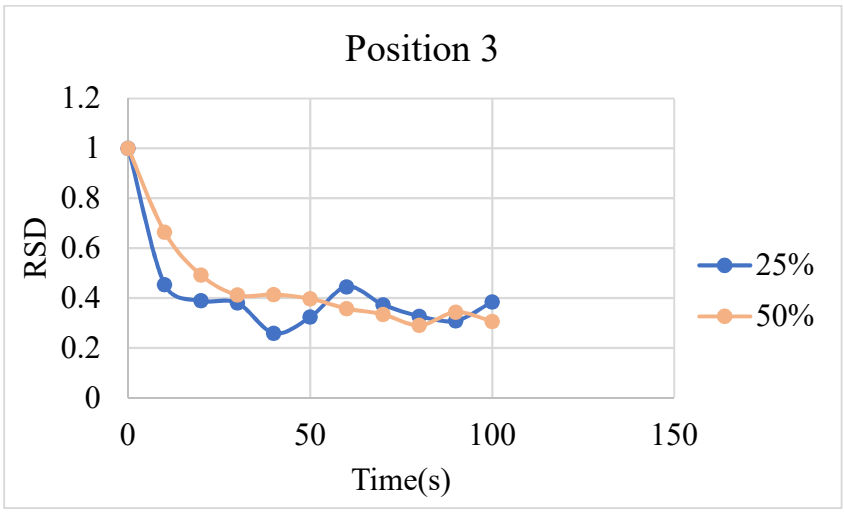

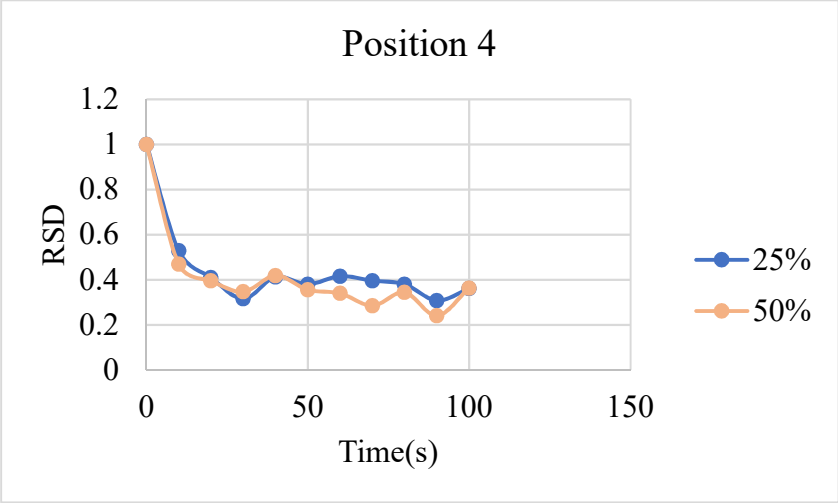

Figure 15: Mixing performance for different fill levels at different baffle positions

It can be observed that with the exception of Position 3, the mixing time for both the 25% and 50% fill level is not very different. This indicates to the fact that we can use higher fill levels with baffles and still maintain a high rate of mixing. This is applicable to many industries where the fill levels are kept very low so as to achieve uniformity throughout the particle bed. Also, the RSD values stabilize around 0.4 and do not go lower for the case of larger particles. This is due to a statistical limitation on the RSD value governed by the size of the particle and the size of the samples being analyzed. This has been well documented in previous studies [45].

3.6 Effect of Particle Size

The effect of particle size on mixing behavior was also studied. Two particle sizes 5mm and 10mm were used. The parameter was then used in combination with different levels of baffle parameters and operation parameters to get a sense of how changing the particle size may affect the mixing behavior. It can be seen in Figs 16(a) and (b) that smaller particles mix faster. This is an apparent contradiction with previous results in the literature. It is

known that axial diffusion and dispersion increase with particle size, so smaller particles will in general, in the absence of baffles, mix slower than larger particles in the axial direction. But since introducing a baffle introduces convective flows in the axial direction, the smaller particles display faster axial mixing than larger particles in a system with baffles. Also, the effect of changing the angle of orientation of the baffle can be seen much clearly when the particle size is smaller. The optimum baffle position changes from Position 3 to Position 4.

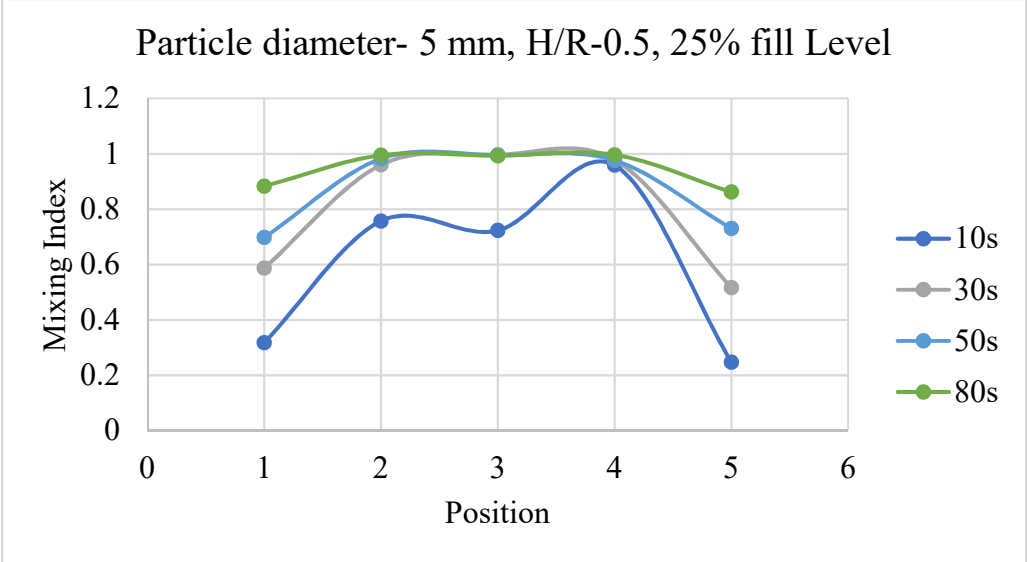

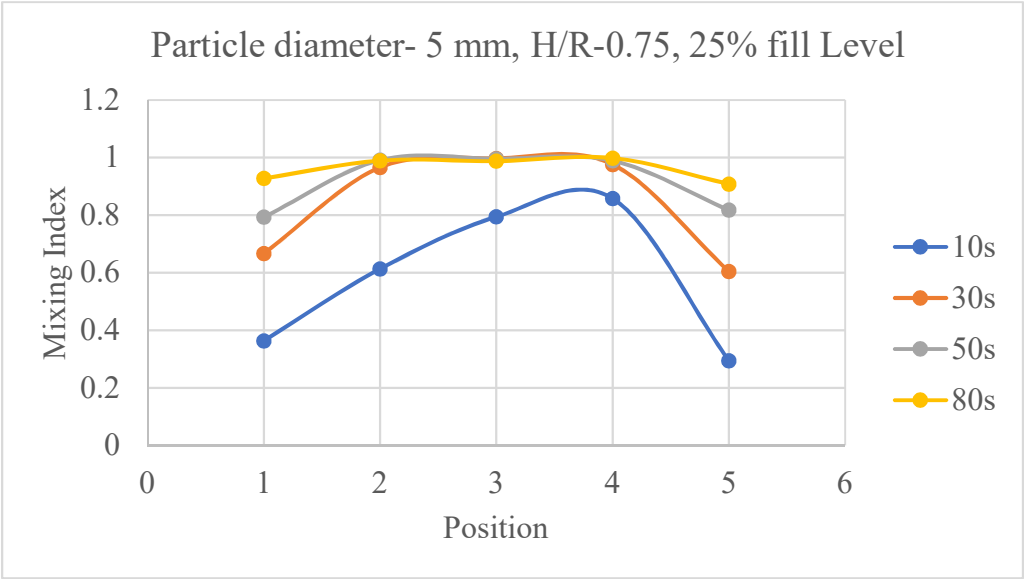

Figure 16. Mixing performance for smaller -particle size

3.7 Simulations with water

The results shown in the previous sections, shed light on how baffles behave in a double cone blender for a mixing case, (ie. in the absence of water or any liquid impregnated on the particle bed.) The next step is now to test the performance of the baffles in the presence of water. In other words, we now wish to understand whether this leads to better axial mixing and water content uniformity in the vessel during the catalyst dry impregnation process. The simulations henceforth involve a spray nozzle. The water transfer algorithm [19] was successfully implemented resulting in a system where several million fluid droplets propagated from a single nozzle into a bed of roughly 10,000–20,000, 5 mm catalyst support particles at 25% fill level. The nozzle was located at the center of the granular bed, spraying approximately 1/3 of the axis diameter (8 cm of 24 cm total). The vessel was rotated at 25rpm. The spray rate from the nozzle was 2.5 liters per hour. The sampling was done at regular time intervals. The samples were taken from 7 bins along the axis of the double cone, as shown in Fig. 2. The average water content for a bin was calculated and then the RSD of water content in a catalyst particle was calculated from the 7 samples.

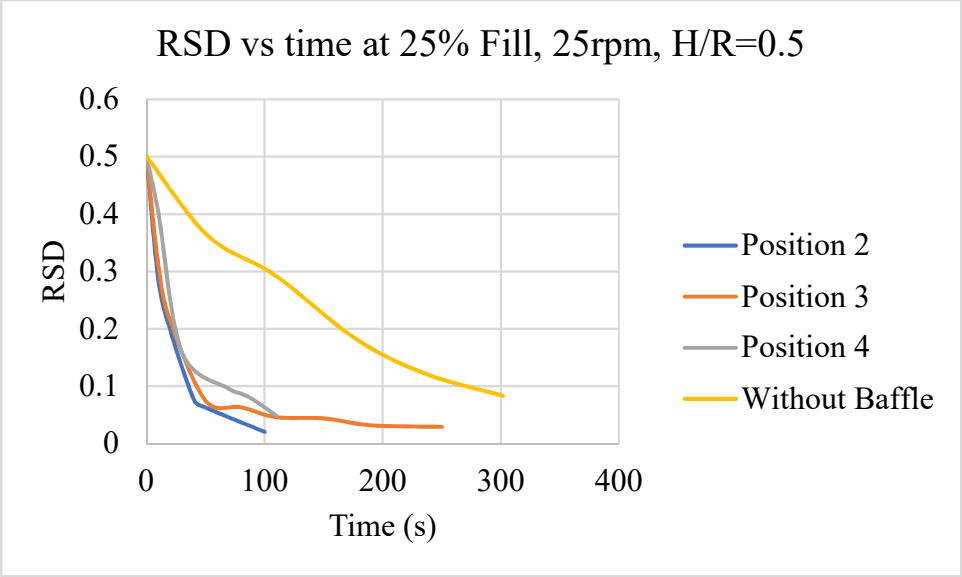

Figure 17. Relative Standard Deviation of the Water Content Uniformity in the particle bed as a function of time for different baffle positions and for the case without any baffles.

Simulations with water spray were then performed to validate the previous results obtained for baffle performance. Position 2 gave the best results (better and faster fluid uniformity in the particle bed) out of the three positions being analyzed but the results for different positions are very close. It is shown that inclusion of baffle can improve the water content uniformity in the particle bed significantly. As shown in the figure, the time for the relative standard deviation (RSD) to reach 0.1 in the case without baffle is more than 250 seconds, but the time for RSD to reach 0.1 in the cases with baffle ranges from 50 to 80 seconds. This is a great improvement in efficiency.

3.8 Flow Analysis

In order to understand the behavior of baffle performance better it is needed to have a better understanding of the flow of particles in the double cone blender. The velocity profile for 10mm particles at 25% fill, 25rpm and for the case of no baffles is analyzed. To do this velocity and position data of the particles is extracted from the EDEM simulation. Since

we desire to analyze the velocity of the particles in the vessel, and the drum rotates at a given speed as well, the data from the EDEM program is given from a stationary reference frame, in other words it contains the resultant velocity of these two components of velocity. So the data needs to be transformed from a stationary to a rotating frame of reference (using Matlab) to obtain the velocity of the moving particles alone (without considering the rpm of the drum). Hence, the velocity of the particles parallel to the surface of the double cone with respect to the surface of the double cone is analyzed; this is shown in Fig 18. Fig 18 shows the velocity profile just as the double cone starts to rotate. The maximum velocity is observed to be just before the flow enters the conical section of the double cone. It then slows down to a minimum in the conical section and then again accelerates down.

The flow profile in the left half of the rotation is almost the same as the right half of the cycle. This is expected as the double cone is a symmetric geometry and the conical sections at the two ends act as nodes [12].

Figure 18 shows the velocity profile of the particle bed in **the absence of baffles** for the left portion of the rotation (left plot in the figure) and for the right half of the rotation (right plot in the figure) as a function of the z coordinate. Notice that the value of the z coordinate goes from 60 to -60 in steps of 20. So, the average value of the velocities for each of these positions were obtained by making an average of the velocities in the particles.

It can be observed that the velocity of the particle bed takes the highest value at the end of the cylindrical section in the absence of baffles. These results in the absence of baffles can shed light on why the baffles at position 3 is the best baffle position as it was seen previously in Figure 12. We argue that this may be because the velocity profile of the

portion of the flow that is interacting with the baffle may be different than that of the whole bed.

To investigate this issue, we did another simulation run, also in the absence of baffles, but this time considering only the particles that would be interacting with the baffle, as if the baffles were put in that location. In other words, only the particles that pass through the region where the baffle is located are considered. For this trial simulations we considered the baffle size ratio equal to H/R=0.5. The results are shown in Fig. 19. In this way, it can be observed that the velocity is the highest around z=0mm i.e. This may explain why when the baffle is located at position 3 the mixing performance is higher that for other positions for H/R=0.5. The hypothesis is that the baffle is breaking the flow at that particular position (z=0). It is worth noticing that the difference between particle velocities across the z axis is not very large for H/R=0.5. Future work needs to be done to test other positions and other baffle ratios.

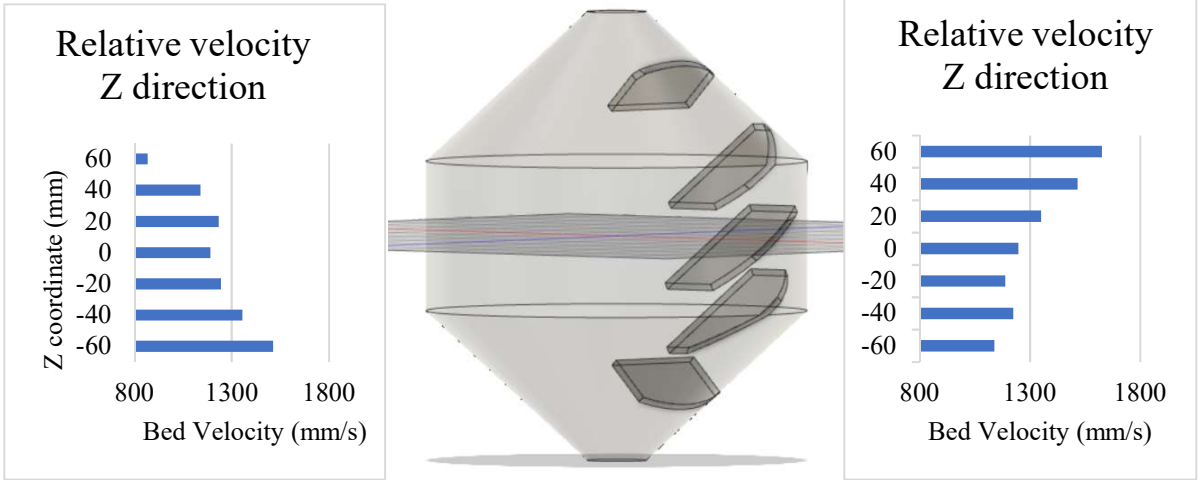

Figure 18. (a) Velocity profile in the absence of baffles for the first half of the rotation of the double cone, (b) Double cone showing the different positions of the baffles and c) velocity profile in the absence of baffles for the second (right half) of the rotation of the double cone.

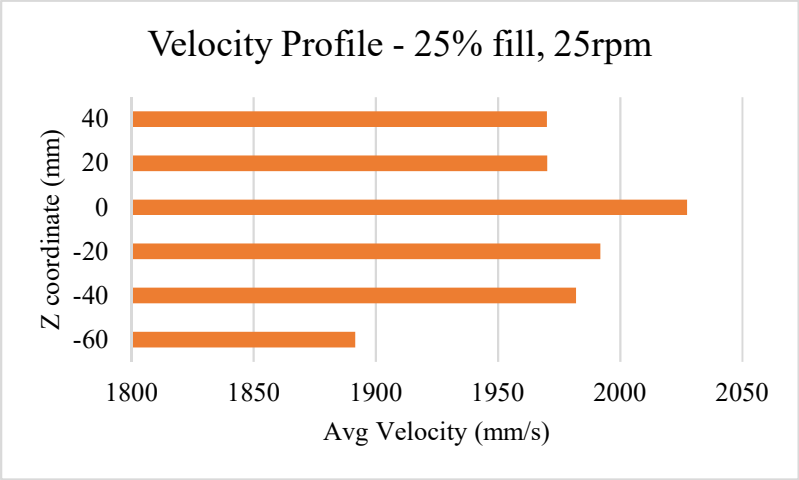

Figure 19. Velocity profile for the bed for H/R=0.5

Chapter 4 - Conclusion

This research was aimed at improving axial mixing in a double cone blender through inclusion of baffles and testing the baffles in the dry impregnation process to improve homogeneity in the particle bed. Several key operation conditions and baffle parameters were identified and examined in detail. During the study it was found that there is an optimal baffle height which offers the fastest mixing rate beyond which, when the baffle size is increased, the mixing performance decreases. Different widths of the baffle were also studied, and it was found that wider baffles perform better but the performance reaches a plateau and there are no further gains for using a wider baffle.

In terms of the angle of orientation of the baffle, while there was no significant difference between different angles for the 10mm particles, an optimal range for the 5mm particles was found within which, the mixing performance was the best in the presence of the baffles. Notice that in the absence of baffles

In terms of the fill level, it was observed that the mixing rate with baffles was almost the same for both fill levels and hence, including baffles can enable the use of much higher fill levels without compromising the mixing rate.

The position 3 (in the middle of the cylindrical section of the geometry) was found to be the best position for 10mm particles at higher ratios of baffle size to particle bed height. When the baffle height is much smaller than the bed height, the position of the baffle has a much smaller impact on the mixing performance. Positions 1 and 5 were the worst positions in all the scenarios that were examined.

Our studies for the effect of the rotational speed confirm previous studies in the literature, (i.e. higher rotational speed led to faster mixing rates). The optimal position of the baffle is position 3 both for low and high rotational speed.

The dry impregnation process with water was also studied in the presence of baffles. Baffles were placed at positions 2, 3 and 4 to examine the effect of baffles in the water content uniformity in the particle bed in the dry impregnation process. All three baffle positions offer much better mixing than no baffles but all of them are very similar in performance and cannot be differentiated. To have a better understanding of all the results, the velocity field in the double cone vessel was calculated and averaged over time. The results of this analysis although not conclusive, they do point out the potential of a procedure to designing baffles by analyzing the velocity profile of the flow in a rotating vessel. We confirmed that hypothesis that when the baffles are located in the regions of higher flow the mixing performance seems to increase. More studies need to be performed to have a more definitive conclusion about this hypothesis.

References

1. Song, G.-M., W.-J. Li, and Y. Zhou, *Synthesis of Mg-doped LiMn2O4 powders for lithium-ion batteries by rotary heating.* Materials chemistry and physics, 2004. **87**(1): p. 162-167.
2. Chang, P.-K. and Y.-N. Peng, *Influence of mixing techniques on properties of high performance concrete.* Cement and Concrete Research, 2001. **31**(1): p. 87-95.
3. Hersey, J., *Powder mixing: theory and practice in pharmacy.* Powder Technology, 1976. **15**(2): p. 149-153.
4. Moskalyk, R., et al., *Uniformity of drug dosage in compressed tablets.* Journal of pharmaceutical sciences, 1961. **50**(8): p. 651-657.
5. Assaf, E.M., L.C. Jesus, and J.M. Assaf, *The active phase distribution in Ni/Al2O3 catalysts and mathematical modeling of the impregnation process.* Chemical Engineering Journal, 2003. **94**(2): p. 93-98.
6. Bornhorst, M., et al., *Influence of pore structure and impregnation-drying conditions on the solid distribution in porous support materials.* Drying Technology, 2016. **34**(16): p. 1964-1978.
7. Gibson, E.K., et al., *Noninvasive Spatiotemporal Profiling of the Processes of Impregnation and Drying within Mo/Al2O3 Catalyst Bodies by a Combination of X-ray Absorption Tomography and Diagonal Offset Raman Spectroscopy.* Acs Catalysis, 2013. **3**(3): p. 339-347.
8. Lekhal, A., B.J. Glasser, and J.G. Khinast, *Impact of drying on the catalyst profile in supported impregnation catalysts.* Chemical Engineering Science, 2001. **56**(15): p. 4473-4487.
9. Lekhal, A., B.J. Glasser, and J.G. Khinast, *Influence of pH and ionic strength on the metal profile of impregnation catalysts.* Chemical Engineering Science, 2004. **59**(5): p. 1063-1077.
10. Li, B.T., et al., *Alumina supported Ni and Co catalysts modified by Y2O3 via different impregnation strategies: Comparative analysis on structural properties and catalytic performance in methane reforming with CO2.* International Journal of Hydrogen Energy, 2016. **41**(33): p. 14732-14746.
11. Schwarz, J.A., *THE ADSORPTION IMPREGNATION OF CATALYTIC PRECURSORS ON PURE AND COMPOSITE OXIDES.* Catalysis Today, 1992. **15**(3-4): p. 395-405.
12. van Dillen, A.J., et al., *Synthesis of supported catalysts by impregnation and drying using aqueous chelated metal complexes.* Journal of Catalysis, 2003. **216**(1-2): p. 257-264.
13. *Handbook of Industrial Mixing: Science and Practice*, ed. E.L. Paul, V. Atiemo-Obeng, and S.M. Kresta. 2003: Wiley.
14. Santos, D.A., et al., *Investigation of particle dynamics in a rotary drum by means of experiments and numerical simulations using DEM.* Advanced Powder Technology, 2016. **27**(2): p. 692-703.
15. Pasha, M., et al., *Effect of particle shape on flow in discrete element method simulation of a rotary batch seed coater.* Powder Technology, 2016. **296**: p. 29-36.
16. Ottino, J., *Mixing, chaotic advection, and turbulence.* Annual Review of Fluid Mechanics, 1990. **22**(1): p. 207-254.

17. Ottino, J. and D. Khakhar, *Mixing and segregation of granular materials.* Annual Review of Fluid Mechanics, 2000. **32**(1): p. 55-91.
18. Alexander, A.W., T. Shinbrot, and F.J. Muzzio, *Granular segregation in the double-cone blender: transitions and mechanisms.* Physics of Fluids, 2001. **13**(3): p. 578-587.
19. Moakher, M., T. Shinbrot, and F.J. Muzzio, *Experimentally validated computations of flow, mixing and segregation of non-cohesive grains in 3D tumbling blenders.* Powder Technology, 2000. **109**(1-3): p. 58-71.
20. Sethuraman, K. and G. Davies, *Studies on solids mixing in a double-cone blender.* Powder Technology, 1972. **5**(2): p. 115-118.
21. Chester, A.W., et al., *Mixing dynamics in catalyst impregnation in double-cone blenders.* Powder Technology, 1999. **102**(1): p. 85-94.
22. Soni, R.K., et al., *Numerical analysis of mixing of particles in drum mixers using DEM.* Advanced Powder Technology, 2016. **27**(2): p. 531-540.
23. Wang, R.H. and L.T. Fan, *Methods for scaling-up tumbling mixers.* Chemical Engineering, 1974. **81**(11): p. 88-94.
24. Brone, D. and F. Muzzio, *Enhanced mixing in double-cone blenders.* Powder Technology, 2000. **110**(3): p. 179-189.
25. Romanski, F.S., et al., *Dry catalyst impregnation in a double cone blender: A computational and experimental analysis.* Powder technology, 2012. **221**: p. 57-69.
26. Shen, Y., W.G. Borghard, and M.S. Tomassone, *Discrete element method simulations and experiments of dry catalyst impregnation for spherical and cylindrical particles in a double cone blender.* Powder Technology, 2017. **318**: p. 23-32.
27. Chalermsinsuwan, B., T. Samruamphianskun, and P. Piumsomboon, *Effect of operating parameters inside circulating fluidized bed reactor riser with ring baffles using CFD simulation and experimental design analysis.* Chemical Engineering Research & Design, 2014. **92**(11): p. 2479-2492.
28. Furukawa, H., et al., *Effects of Location of Baffle and Clearance between Baffle and Vessel Wall on Isolated Mixing Regions.* Journal of Chemical Engineering of Japan, 2018. **51**(1): p. 29-32.
29. Liu, B.Q., et al., *CFD SIMULATION OF THE MIXING AND DISPERSING OF FLOATING PARTICLES IN A VISCOUS SYSTEM.* Brazilian Journal of Chemical Engineering, 2017. **34**(4): p. 1175-1189.
30. Liu, Y.F., et al., *CFD study on the effect of baffle arrangements on flow patterns in tubular membrane channel.* Desalination and Water Treatment, 2017. **75**: p. 10-17.
31. Ramsay, J., et al., *Mixing of Newtonian and viscoelastic fluids using "butterfly" impellers.* Chemical Engineering Science, 2016. **139**: p. 125-141.
32. Satjaritanun, P., et al., *Experimental and computational investigation of mixing with contra-rotating, baffle-free impellers.* Chemical Engineering Research & Design, 2018. **130**: p. 63-77.
33. Xu, B.P., et al., *Numerical Simulation of Chaotic Mixing in Single Screw Extruders with Different Baffle Heights.* International Polymer Processing, 2016. **31**(1): p. 108-118.
34. Xu, B.P., et al., *Enhancement of mixing by different baffle arrays in cavity flows.* Chemical Engineering Science, 2015. **137**: p. 837-851.

35. Xu, B.P., et al., *Evaluation of Mixing Performance in Baffled Screw Channel Using Lagrangian Particle Calculations.* Advances in Polymer Technology, 2017. **36**(1): p. 86-97.
36. Yu, F.H., et al., *Enhanced axial mixing of rotating drums with alternately arranged baffles.* Powder Technology, 2015. **286**: p. 276-287.
37. Zhou, E.H., et al., *Fluidization characteristics and fine coal dry beneficiation using a pronation-grille baffle dense phase medium fluidized bed.* Fuel, 2016. **185**: p. 555-564.
38. Zhou, Z.X., et al., *Enhancing mixing of cohesive particles by baffles in a rotary drum.* Particuology, 2016. **25**: p. 104-110.
39. Cundall, P.A. and O.D.L. Strack, *A discrete numerical model for granular assemblies.* Geotechnique, 1979. **29**: p. 47–65.
40. Hertz, H., *On the contact of elastic solids.* Journal fur die reine und angewandte Mathematik 1882. **92**: p. 156-171.
41. Tsuji, Y., T. Tanaka, and T. Ishida, *LAGRANGIAN NUMERICAL-SIMULATION OF PLUG FLOW OF COHESIONLESS PARTICLES IN A HORIZONTAL PIPE.* Powder Technology, 1992. **71**(3): p. 239-250.
42. Mindlin, R.D. and H. Deresiewicz, *Elastic spheres in contact under varying oblique forces.* Journal of Applied Mechanics, 1953. **20**.
43. Lacey, P.M.C., *Developments in the theory of particle mixing.* Journal of applied chemistry, 1954. **4**(5): p. 257-268.
44. Cullen, P.J., *Food mixing: Principles and applications*. 2009: John Wiley & Sons.
45. Lekhal, A., et al., *Characterization of granular flow of wet solids in a bladed mixer.* Aiche Journal, 2006. **52**(8): p. 2757-2766.